Desalination and Water Treatment
www.deswater.com

doi: 10.5004/dwt.2020.25142

181 (2020) 376–384
March

Isotherm, kinetic and thermodynamic studies for adsorption of lead(II) onto modified Aloji clay

K.S. Obayomi[a,*], M. Auta[b], A.S. Kovo[b]

[a]*Department of Chemical Engineering, College of Engineering, Landmark University Omu-Aran Kwara State, Nigeria, Tel. +2348066967564; emails: obayomi.kehinde@lmu.edu.ng*
[b]*Department of Chemical Engineering, Federal University of Technology Minna, Niger State, Nigeria, email: manaseauta@yahoo.com (M. Auta), kovo@futminna.edu.ng (A.S. Kovo)*

Received 24 June 2019; Accepted 9 November 2019

ABSTRACT

This study utilized Aloji clay modification for Pb(II) adsorption from an aqueous solution via batch adsorption process. The clays were characterized by X-ray fluorescence, X-ray diffraction, Fourier transform infrared spectroscopy, scanning electron microscopy and Brunauer–Emmett–Teller (BET). The raw clay and acid-activated clay have BET surface areas of 138.7 and 172.0 m^2/g, respectively. The adsorption parameters: adsorbent time, dosage, temperature, pH, and initial concentration were all investigated. Out of the three isotherm models investigated, the Freundlich model gave the best fit to the experimental data. The result of kinetic and thermodynamic studies revealed that the adsorption process obeyed pseudo-second-order, spontaneous, endothermic, and physical progression. The adsorption of Pb(II) onto activated Aloji clay, when compared with other natural adsorbents from literature, gave the highest monolayer adsorption capacity.

Keywords: Aloji; Pb(II); Isotherm model; Kinetics; Thermodynamics

1. Introduction

One of the most vital resources essential for the survival of living organisms in the entirety of the world is water. According to recent research, water covers about 70% of the earth, out of which, 2.5% is seen as clean water and the residual is treated and recycled so they can be reused. The use of water is not only restricted to domestic purposes, but it can also be used in a broader spectrum, particularly in the agricultural and industrial sectors [1]. The quality of water has degraded rapidly due to the diverse release of inorganic and organic pollutants, emanating from human influences on nature and other natural sources. Recently, the contamination of water bodies' through fishing, recreation, transportation, domestication, and commercial activities has become major sources of concern, as it affects the survival of living organisms [2].

Heavy metals, among other pollutants, are the most hazardous due to their toxic nature [3]. When wastewater from electroplating, mining, tanneries, fertilizer, painting, and batteries industries containing heavy metals are discharged, they flow into rivers, streams, and lakes making them unhealthy for consumption. Heavy metals, directly or indirectly enter water bodies at a concentration which is beyond the acceptable threshold limit [4–6]. These are highly toxic and stay longer in various oxidation states in the environment.

Numerous technologies have been used for the removal of heavy metals from wastewater; however, their disadvantages among several others include sludge generation in large amounts, low removal efficiency, high cost of equipment maintenance, high operational cost, removal of partial metal ion, high energy requirement and cost of equipment [7]. Furthermore, the new emergence technique which is seen

* Corresponding author.

as a potential alternative to other technologies for heavy metals removal is adsorption. Adsorption offers better capacity in terms of pollutant recovery possibility, efficiency, cost-effectiveness, and easy handling [8].

Clays, in recent years, have gained great attention as a result of their availability, wide application range and best replacement for high-cost commercial adsorbents used in adsorption processes. Among other methods of clay beneficiation for adsorption processes, acid treatment in its best form has yielded excellent results in producing clay adsorbent [9]. Clay has broad benefits and utilities when compared with other commercial adsorbents, some of which include excellent specific surface area, high mechanical and chemical stability, availability, affordability, ion exchangeability, surface, and structural properties variety, as well as good adsorption capacities [10].

This experimental study is aimed at the abundant potentials found in clay obtained from Aloji in Kogi State of Nigeria as a possible replacement to other commercial adsorbents for Pb(II) adsorption from an aqueous solution. Although researchers have carried out numerous studies on clay activation for heavy metals uptake, none have however reported to the use of Aloji clay modification using H_2SO_4 as an activating agent for Pb(II) uptake to the best of our knowledge.

2. Materials and method

2.1. Materials

Analytical grade $Pb(NO_3)_2$ and H_2SO_4 used for this experimental work were supplied by Merck Chemical Company, U.K. The local clay that was used for this research was collected from Aloji in Kogi State, Nigeria. The parent clay (PC) was crushed, grounded, and reduced to a particle size of 125 μm mesh at 120°C in an electric oven. Afterward, it was then dried for 4 h.

2.2. Clay treatment

The dried, powdered PC was purified and activated in a 250 mL Erlenmeyer beaker on a hotplate magnetic stirrer with 1.5 M H_2SO_4, clay/acid ratio of 1 g/100 mL. The desired mixture temperature was set at 100°C and vigorously stirred for 2 h. After clay activation, the mixture was washed severely with distilled water to achieve neutrality (pH 6.8–7), and after washing, it was filtered, oven-dried for 4 h at 108°C and then stored for further use in an airtight container.

2.3. Clay characterization

X-Ray fluorescence (XRF), Fourier transform infrared spectroscopy (FT-IR), X-ray diffraction (XRD) analysis Brunauer–Emmett–Teller (BET) and scanning electron microscopy (SEM) have been described to determine the elemental composition, surface chemistry, surface area and pore volume, structural morphology, and crystal structure respectively. The XRF assessment of the clay samples was recorded using a Model-PW2400 Phillips, USA. FT-IR spectra were registered by Perkin-Elmer infrared spectrophotometer, USA. The surface area and porosity characterizations were performed using BET (Micrometrics ASAP 2020), USA. The morphological structures were determined using the microanalysis scheme Oxford INCA/ENERGY-350, UK and the identification of the powdered clay material in the crystal phase was performed using a Bruker AXS D8 X-ray diffractometer system, USA.

2.4. Batch adsorption studies

Batch equilibrium studies with different Pb(II) concentrations (30–150 mg/L) in a collection of 250 mL Erlenmeyer flasks at various temperatures (30°C, 40°C and 50°C), were conducted. 0.1 g of activated Aloji clay (AAC) was measured into each flask and the Pb(II) solution initial pH was maintained throughout the experiment. Thereafter, the flasks were placed in isothermal water bath shaker for 2 h agitation at a controlled temperature of 30°C, with 140 rpm shaker speed for equilibrium attainment. Prior to equilibrium attainment, samples at different intervals of time were taken, filtered and analyzed with the aid of atomic absorption spectroscopy (PinAACLE 900Z, U.S.) to determine the unadsorbed Pb(II) in the solution. The isothermal shaker was attuned to 40°C and 50°C and with another set of flasks; the entire adsorption process was repeated. At equilibrium, the adsorbed amount of Pb(II) was determined by:

$$q_e = \frac{\left(C_0 - C_e\right)V}{W} \tag{1}$$

where C_e and C_0 are the Pb(II) equilibrium and initial concentration (mg/L); V (L) is the adsorbate volume L; W is the weight of the adsorbent (g).

The kinetic adsorption studies of Pb(II) onto AAC were investigated at a time fixed interval. The adsorbed amount at time t of Pb(II) was given as:

$$q_t = \frac{\left(C_0 - C_t\right)V}{W} \tag{2}$$

where C_t is Pb(II) concentration at any time (mg/L).

This experiment was carried out using a set of Erlenmeyer flasks (250 ML) containing 150 mg/L of Pb(II). 50 mL of NaCl was poured in each of the flasks and the pH was varied (pH 2–11) by adding 0.1 M NaOH or 0.1 M HCL. In each flask, 0.1 g of the adsorbent prepared (AAC) were added and stirred vigorously in a water bath isothermal shaker for 24 h at 50°C. The final pH after 24 h was determined and the pH_{final} graph was plotted against $pH_{initial}$ and the pH_{pzc} value was obtained from the plot.

3. Results and discussion

3.1. XRF techniques

The elemental composition of PC and AAC from XRF analysis carried out is depicted in Table 1. Results revealed that the PC and AAC contained in major quantities silica and alumina as oxides of magnesium, calcium, potassium, iron, and tin are available in traceable amounts.

The result as revealed shows changes in the elemental composition of PC after treatment with acid when compared

It was observed that after acid modification, there was a rise in SiO_2 and decrease in Al_2O_3, MgO, CaO and K_2O, as TiO_2 remains unchanged [11]. The elemental analysis prominently shows that during acid treatment, the octahedral layer attack occurs in the leaching process, which resulted in alumina content decrease as a result of Al^{3+} ion leaching due to hydrolysis under acidic conditions from the octahedral layer [12].

Table 1
XRF analysis of PC and AAC

Elemental oxides	PC	AAC
SiO_2	49.90	59.81
Al_2O_3	31.20	24.32
Fe_2O_3	0.90	0.66
K_2O	1.38	1.20
TiO_2	0.20	0.20
CaO	0.60	0.56
MgO	0.40	0.27
Loss on Ignition	15.0	9.90

3.2. FT-IR analysis

PC and AAC FT-IR spectra and associated assignment bands are presented in Fig. 1 and Table 2. The spectra indicate different numbers of adsorption peaks in the range of 500–4,000 cm^{-1}, which was displaced reflecting the complex nature of the clay. A comparison of PC and AAC from the obtained results shows that some peaks have shifted or disappeared and new ones were formed.

The PC and AAC showed two important bands in the stretching region of O–H at 34,214.83 and 3,414.12 assigned to Al–OH (stretching), lying between the octahedral sheet, and the structural hydroxyl groups. The quantity of physical water on the clay surface could be ascribed to the band observed at 3,294.83 on the AAC spectrum. Similarly, the bands at 1,637.62 and 1,647.26 on PC and AAC in the bending region respectively, were assigned to H–O–H bending (physisorbed). The absorption band at 1,541.18 and 1,384.94 of the AAC were attributed to Al–Al–OH and Si–O–Al stretching [14,17]. While the Si–O stretching was ascribed to the infrared (IR) band at 1,041.60. Furthermore, the AAC various functional groups were as a result of the PC modification with

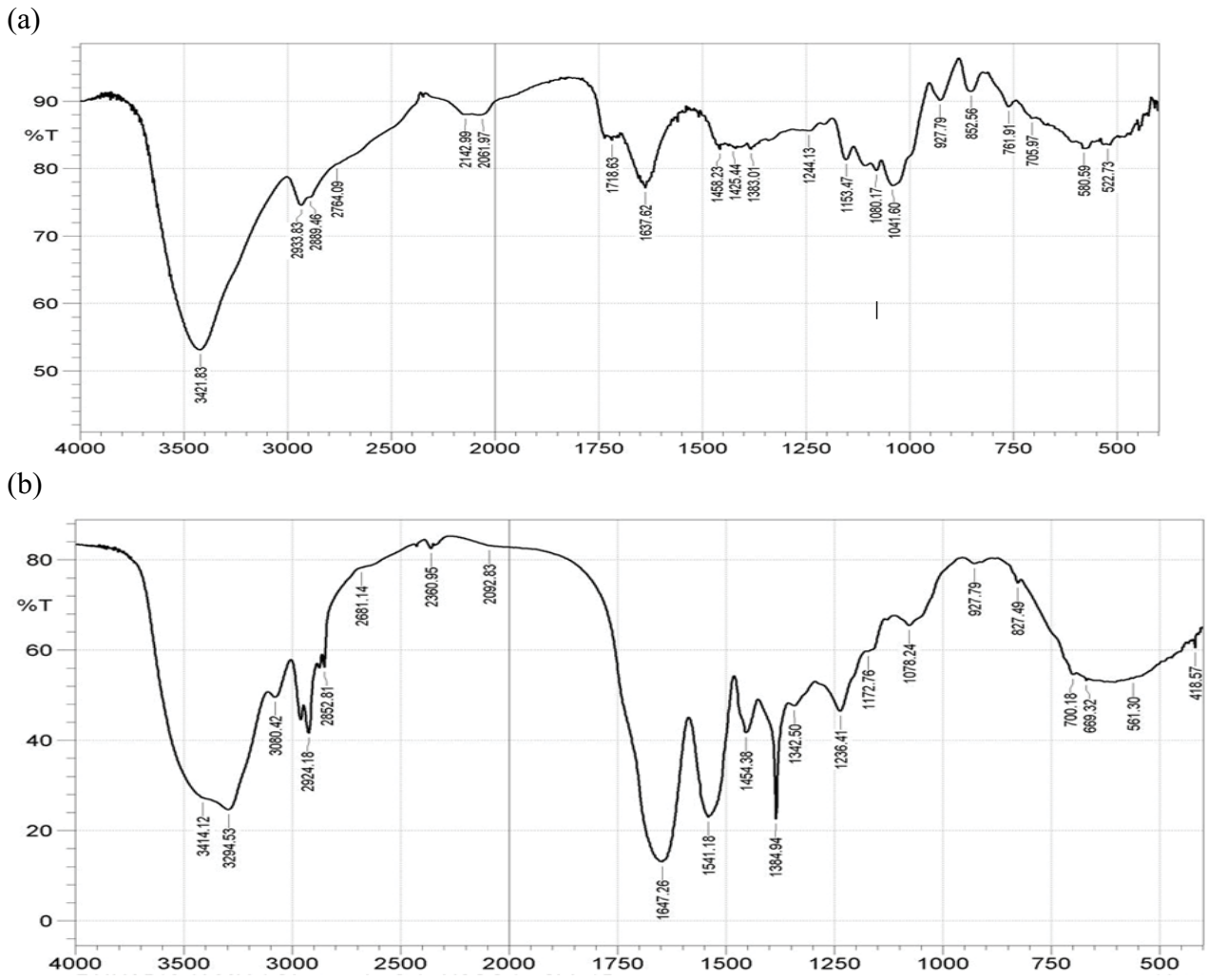

Fig. 1. IR spectrum for (a) PC and (b) AAC.

Table 2
IR bands for PC and AAC with their assignments [13–16]

Bands (cm^{-1})	Assignments
1,637.62 and 1,647.26	$H–O–H_{bending}$ (physisorbed)
1,384.94	$Si–O–Al_{str}$
1,541.18	$Al–Al–OH_{str}$
1,041.60	$Si–O_{str}$
3,294.83	$Al–O–H_{str}$ (physisorbed water)
3,414.12 and 3,421.83	$Al–O–H_{str}$ (structural hydroxyl groups, octahedral)

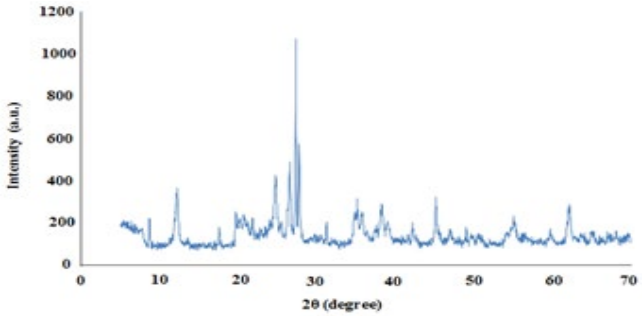

Fig. 2. XRD patterns of AAC.

an acid, which contributed greatly to its huge adsorption of Pb(II) from wastewater [18,19].

3.3. BET analysis

The BET surface analysis provided a clear picture of the adsorbent surface area, pore-volume, and size. PC and AAC BET surface areas were 138.70 and 172 m^2/g; a total pore volume of 0.0711 and 0.088 cc/g, and a pore size of 1.17 and 1.27 nm, respectively. The pore volume, surface area and pore size increase as regards AAC, which may result from the clay acid treatment which can be attributed to cation exchange and more silica formation [20].

3.4. XRD investigation

The XRD results depicted in Fig. 2 indicated that Bragg's angles (2θ) of 12.35°, 19.89°, 20.38°, 24.88°, 34.94°, 35.95°, 36.06°, 38.35°, 45.24°, 54.88°, and 62.37° were present in the AAC sample. The peak positions were also used together with crystallite sizes to match the phases with their corresponding sizes as reported in the literature. The peak at 26.65° was due to crystalline silica, also known as quartz with the highest intensity of about 1,000 counts, whereas the other peaks which represented the AAC mineral were much lower – they generally had an intensity of about 400 counts and even lower.

This result can be ascribed to the greater quartz material that provides the AAC the attribute to be used as a better adsorbent for Pb(II) uptake. The Debye-Scherrer equation shown in Eq. (3) was applied to the XRD peak sharp to obtain crystallite sizes. The result showed that the AAC was nanopoly crystalline, with ranging sizes from 24–114 nm. The crystallite means size of 41.64 nm obtained indicated that the clay was characteristically a highly crystalline material [21].

$$D = \frac{K\lambda}{\beta\cos\theta} \tag{3}$$

where D is the particle diameter, λ is the wavelength (0.1541 nm), θ is the angle of diffraction, K is the Scherrer constant (0.94) and β is the full width at half maximum.

3.5. Morphological structure of PC and AAC

The SEM image carried out on PC and AAC are presented in Fig. 3 in other to further clarify the adsorption of Pb(II) onto AAC. The result showed that PC had plate-like sheet morphology before activation and after the chemical activation process with sulphuric acid. The structure was partially destroyed with widen pores. The porous structure and surface area of the AAC, are thus enhanced.

3.6. pH effect

An important parameter that needs to be considered when determining metal ion removal percentage is the study of pH. It helps to measure the acidity and basicity of the adsorption processes. Pb(II) solution pH was varied between the ranges of pH 2–11 as shown in Fig. 4. A careful

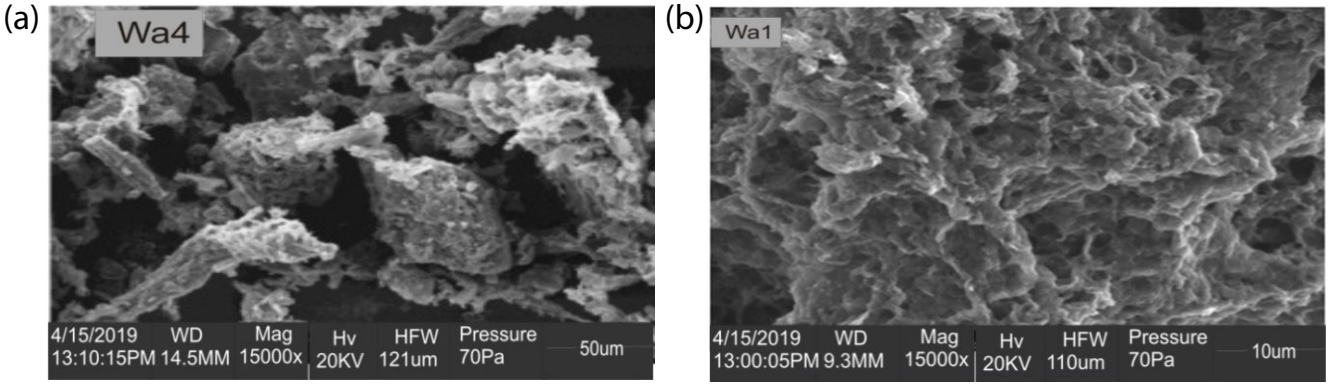

Fig. 3. SEM analysis on (a) PC and (b) AAC.

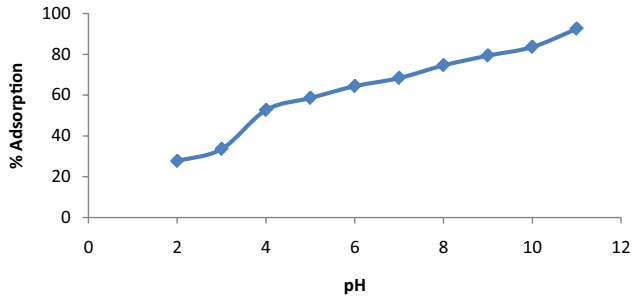

Fig. 4. pH effect on Pb(II) removal onto AAC.

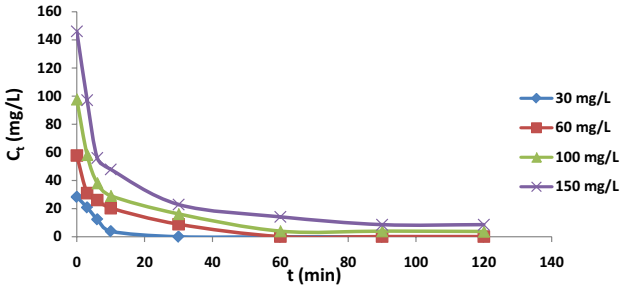

Fig. 5. Initial concentration effect of Pb(II) onto AAC at 50°C.

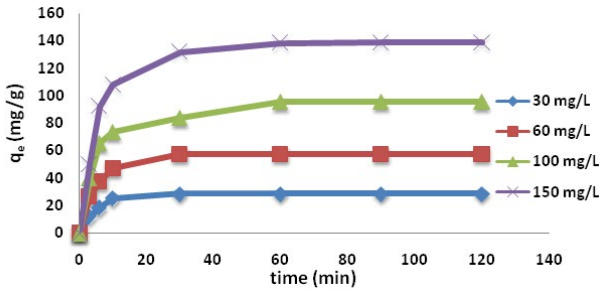

Fig. 6. Contact time effect on the uptake of Pb(II) onto AAC at 50°C.

observation of the pH solution that was studied showed that at lower pH (below 4), there was little uptake of Pb(II). This fact can be accredited to more hydrogen ion (protonated) formation. Thus, influencing the adsorbent sites to be charged positively resulting in electrostatic repulsion between adsorbent sites (positively charged) and metal ion (positively charged) [22]. A higher removal percentage of Pb(II) was attained at an increased pH (above 5). This can be attributed to less formation of hydrogen ion (deprotonated), making the adsorbents surface more negatively charged thereby promoting an electrostatic attraction between negatively charged adsorbent sites and positively charged metal ion [9,23]. The pH at point zero charges (pH_{pzc}) can be described as a point where the net surface charges are zero. The pH_{pzc} of AAC was examined from the plot of pH_{final} against $pH_{initial}$ as 5.7 (Fig. not shown) indicating that at pH (<4) the adsorbent site is charged positively while at (>5) the surface is charged negatively (deprotonation) thus, favoring the uptake of Pb(II). Besides, a pH of 5.7 was used throughout the whole experiment.

3.7. Effect of contact initial concentration of Pb(II)

The effect of contact time and initial concentration of Pb(II) removal onto AAC are depicted in Figs. 5 and 6. These were measured based on the equilibrium position attainment between Pb(II) and the adsorbent produced (AAC)– that is the state at which the adsorbing and the desorbing amount of Pb(II)on the adsorbent are in an equilibrium dynamic state. Pb(II) adsorption onto AAC as shown by the plots, was seen to have propagated gradually with a successive initial Pb(II) concentration increase. Thus, the adsorption extent decreased with the increase in metal ion loading [22]. At a lower concentration of Pb(II) solution, maximum adsorption capacity (q_e) was more rapid than at concentration higher. This finding was ascribed to the proportionate amount of vacant sites at those reduced levels of molecules of the adsorbate, which could also have led to the fast Pb(II) removal at the early stage of the adsorption process [24].

The results also revealed that at lower Pb(II) concentration, equilibrium position was faster attained with lesser time, while longer time was seen for equilibrium attainment at higher Pb(II) concentration as illustrated in Fig. 6. The equilibrium attainment at a longer time of higher initial Pb(II) concentration, could be attributed to the molecular queue before saturation waiting to be adsorbed at a constant adsorbent dosage, with few vacant sites and adsorbent molecules movement to the outer surface of the molecules, through diffusion into the adsorbent pores [25].

3.8. Effect of dosage

This study examined the effect of adsorbent dosage on Pb(II) uptake by varying 0.1 to 1 g/L of the adsorbent (AAC) with constant Pb(II) concentration (150 mg/L) for 60 min at 323 K. It was revealed from the graph (Fig. 7), that the uptake of Pb(II) increased with adsorbent dosage increase. However, the AAC dosage increase from 0.1 to 0.7 g/L, gave a rapid uptake of Pb(II) while further increment beyond this point (>7), does not lead to a significant increase in the adsorption of Pb(II). Also, an increase in the proportion of Pb(II) removal could be as a result of more active sites present on the AAC; metal ions at lower adsorbent dosage with limiting adsorption sites compete for adsorption [26].

3.9. Isotherm studies

The experimental data obtained from dynamic equilibrium for Pb(II) adsorption onto AAC were widely fitted to three isotherms namely, Temkin, Freundlich, and Langmuir. The linearized form of the Langmuir isotherm is calculated as [27]:

$$\frac{C_e}{q_e} = \frac{1}{q_{\max} K_L} + \frac{C_e}{q_{\max}} \tag{4}$$

where q_e is the amount of Pb(II) adsorbed at equilibrium (mg/g); $q_{\max}$ is maximum adsorption capacity of Pb(II) (mg/g); C_e is metal ion concentration at equilibrium (mg/L).

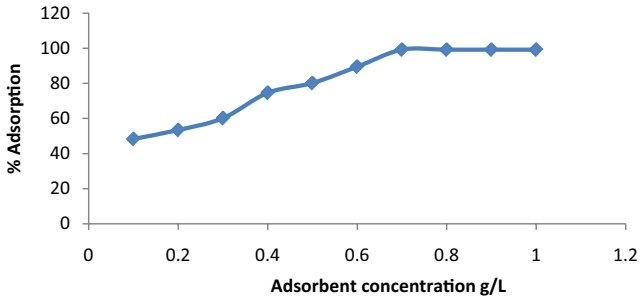

Fig. 7. Adsorbent dosage effect on the removal of Pb(II) onto AAC.

Freundlich model presumes a surface heterogeneous energy adsorption, and the linearized form for the equation is evaluated as [28]:

$$\log q_e = \log K_F + \frac{1}{n}\log C_e \quad (5)$$

where K_F and n are the Freundlich coefficient; n gives favourability information on the adsorption process while K_F is the adsorption capacity of the Pb(II).

The effect of adsorption on the adsorbate interaction was further considered using the Temkin isotherm model and the linearized form of the equation is given as [29]:

$$q_e = B \ln A_T + B \ln C_e \quad (6)$$

where A_T is the binding equilibrium constant relating to the maximum binding, B is the adsorption energy.

$$B = \frac{RT}{b_T} \quad (7)$$

where $1/b_T$ indicated the adsorption potential of the adsorbent, R is the gas universal constant (8.314 J/Kmol) and T is the temperature in Kelvin.

The Pb(II) adsorption onto AAC studied by the three adsorption isotherm models well described the process adsorption with theoretical parameters along with regression coefficients and some variance level in their fitness as shown in Table 3 and Fig. 8.

The isotherm best fit was chosen as informed by the highest coefficient of R^2 value; how close to 1 describing the model fitness to the experimental data. The result revealed that Freundlich gives the best fit and was closely followed by Langmuir and Temkin respectively as seen in their larger R^2 values [25]. The adsorption monolayer capacity of 172.857 mg/g as informed by Langmuir model shows that on the adsorbent surfaces there was Pb(II) monolayer coverage. Result also revealed that the Langmuir constant affinity (K_L) for adsorption decreases as the temperature is increased [30]. However, the best fit Freundlich isotherm model shows favorable Pb(II) adsorption of on the adsorbent heterogeneity surface which was observed from the condition of the value of $0 < 1/n < 1$ satisfying the favourability and heterogeneity of the model. The Temkin model revealed the interaction between the Pb(II) and the adsorbent and also, the extent of

Table 3
Adsorption isotherm models parameter on Pb(II) adsorption onto AAC

Isotherms	Parameters	30°C	40°C	50°C
Langmuir	q_{max} (mg/g)	142.857	166.667	172.857
	K_L (L/g)	0.571	0.429	0.40
	R^2	0.914	0.927	0.945
Freundlich	K_F	71.780	76.033	79.250
	$1/n$	0.277	0.235	0.219
	R^2	0.984	0.999	0.995
Temkin	A_T (L/mg)	78.54	246.165	478.531
	b_T (KJ/mol)	131.823	164.597	184.185
	R^2	0.829	0.800	0.896

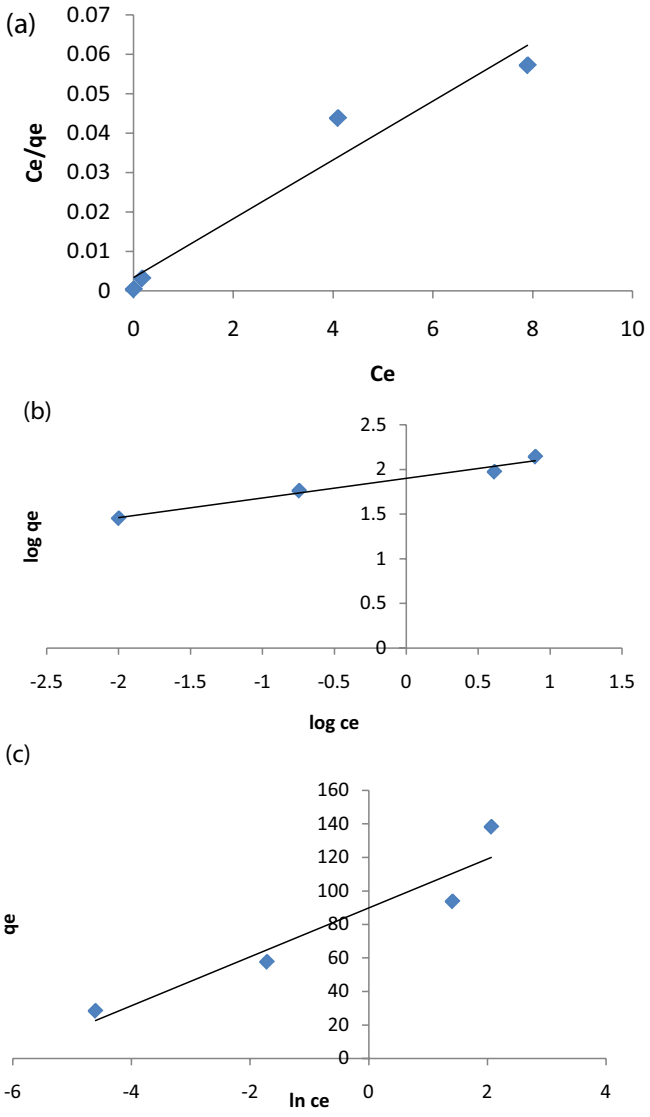

Fig. 8. Plots of (a) Langmuir, (b) Freundlich, and (c) Pb(II) adsorption onto AAC at 50°C.

binding energies uniform distribution which may depend on the functional group's distribution of Pb(II), adsorbent surface (AAC) and their density [22].

The maximum monolayer adsorption capacity of Pb(II) onto different adsorbent were compared to the present studies (Table 4).

3.10. Kinetic studies

The pseudo-first-order model linearized form of an equation is given as [44]:

$$\log\left(q_e - q_t\right) = \log q_e - \frac{k_1 t}{2.303} \tag{8}$$

q_e and q_t (mg/g) are the amounts at equilibrium and at time t of metal ion adsorbed; k_1 is the rate adsorption constant (min^{-1}).

The linearized pseudo-second-order form is evaluated as [45].

$$\frac{t}{q_t} = \frac{t}{q_e} + \frac{1}{k_2 q_e^2} \tag{9}$$

k_2 is the second-order adsorption constant rate (g/mg min).

The kinetic results of the two models obtained revealed that Pb(II) adsorption on AAC was well described by pseudo-first-order and pseudo-second-order kinetic models but the best description is given by second-order as seen in their adsorption constant rate smaller values and coefficient of regression (R^2) as depicted in Table 5 and Fig. 9. In a comparison of the second-order to that first-order, the result disclosed that second-order R^2 values tend toward unity (>0.90). In addition to this, the adsorption capacities from calculated ($q_{e,cal.}$) values when compared to that of the experimental values ($q_{e,exp.}$) for second-order were very close [46]. The decrease in the rate constant (k_2) for second-order as initial Pb(II) concentration increases revealed that it is faster for the adsorption process to attain equilibrium at a lower concentration. The inability of the first-order to give adsorption process a better description may be attributed to the adsorption process being controlled by boundary layer limitations [47].

3.11. Thermodynamic studies

The values obtained for thermodynamic studies revealed the feasibility and spontaneity of Pb(II) adsorption onto AAC and the equation is expressed as:

Table 4
Pb(II) adsorption capacity onto various adsorbents

Adsorbents	q_{max} (mg/g)	References
Bentonite clay	28.00	[31]
Illite clay	25.44	[32]
Sepiolite clay	30.5	[33]
KC clay	86.40	[34]
Zeolite	24.40	[33]
Paper sludge	103.50	[35]
Montmorillonite clay	37.16	[36]
Zeolite–Kaolin–Bentonite	108.70	[37]
Kaolinite	31.75	[38]
Nano-adsorbent	169.34	[39]
Redox polymer	21.99	[40]
Coconut residue	6.535	[41]
Marula seed	20.00	[42]
Activated carbon (rice husk)	5.348	[43]
Aloji clay	172.86	Present work

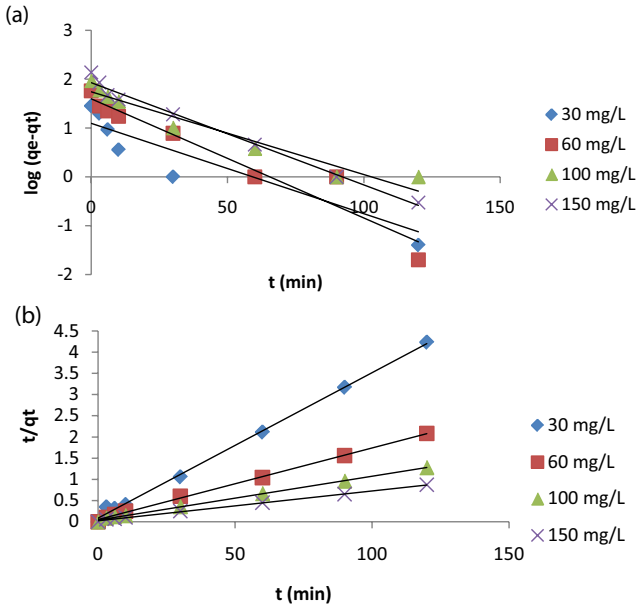

Fig. 9. Plots of (a) pseudo-first and (b) pseudo-second-order kinetic for Pb(II) adsorption onto AAC.

Table 5
Kinetic models parameter for adsorption of Pb(II) onto AAC at 50°C

			Pseudo-first-order			Pseudo-second-order		
Adsorbents	Pb(II) conc. (mg/L)	$q_{e,exp.}$ (mg/g)	$q_{e,cal.}$ (mg/g)	k_1 (min^{-1})	R^2	$q_{e,cal.}$ (mg/g)	k_2 (min^{-1})	R^2
AAC	30	28.34	10.046	0.0253	0.619	29.142	0.0101	0.966
	60	57.60	29.923	0.0345	0.862	62.500	0.00388	0.997
	100	93.70	44.631	0.0392	0.859	100.000	0.00303	0.998
	150	137.50	74.131	0.0392	0.942	142.857	0.00196	0.998

Table 6
Thermodynamics parameters for Pb(II) adsorption onto AAC at various temperatures

Adsorbent	Pb^{2+} conc. (mg/L)	$\Delta H°$ (kJ/mol)	$\Delta S°$ (J/Kmol)	$\Delta G°$ (kJ/mol)			R^2
				30°C	40°C	50°C	
AAC	30	74.884	298.504	–15.562	–18.547	–19.532	0.994
	60	4.534	62.152	–14.298	–14.920	–15.541	0.798
	100	5.807	43.885	–7.480	–7.929	–8.368	0.873
	150	3.735	35.384	–6.986	–7.340	–7.693	0.999

$$\log\frac{q_e}{C_e} = -\frac{\Delta H°}{2.303R}\left(\frac{1}{T}\right) + \frac{\Delta S°}{2.303R} \tag{10}$$

where $\Delta H°$ is the enthalpy change (J/mol) and $\Delta S°$ is the entropy change (J/mol). The graph of log q_e/C_e against $1/T$ gives a linear plot where we obtain both $\Delta S°$ from the slope and ΔH from the intercept. The free Gibbs energy is obtained using this equation:

$$\Delta G° = \Delta H° - \Delta S° \tag{11}$$

The thermodynamic studies of Pb(II) adsorption process parameters as shown in Table 6, revealed that the process was spontaneous as seen in the $\Delta G°$ negative values. The increase in ΔG values with temperature increase implies that higher temperature favors the adsorption process [48]. Positive enthalpy change ($\Delta H°$) values obtained for all temperatures also indicated that the reaction is endothermic. The positive entropy values ($\Delta S°$) also signify a strong affinity between the adsorbed Pb(II) molecules and the AAC resulting in randomness increase at the adsorbent-adsorbate interface during the adsorption process [49,50]. Furthermore, the absolute variation in the ΔG values between –20 to 0 kJ/mol indicates physisorption while chemisorption is between –80 to –400 kJ/mol. Thus, the results obtained revealed that the process adsorption is physical with $\Delta G°$ values less than –20 kJ/mol and involves a weak force of attraction [51–53].

4. Conclusion

A batch adsorption process under study was used to investigate Pb(II) uptake onto AAC. The clay was modified with H_2SO_4 and this improved the surface area from 138.70 to 172.0 m^2/g, and monolayer adsorption capacity of 172.857 mg/g was exhibited by the adsorbent at 50°C. Pb(II) percentage adsorption increased with an increase in pH values. The Pb(II) uptake appreciably depends on the amount of adsorbent. The three isotherm models parameter studied revealed that Freundlich gave the best fit followed by Langmuir and Temkin respectively. The adsorption of Pb(II) onto AAC followed pseudo-second-order, spontaneous, endothermic and physical involving weak forces as revealed by the kinetic and thermodynamic studies. The investigation showed that AAC is effective, efficient, economical and has the potential to be used as an adsorbent for continuous Pb(II) removal from wastewater.

References

[1] T. Saleh, Mercury sorption by silica/carbon nanotubes and silica/activated carbon: a comparison study, J. Water Supply Res. Technol. AQUA, 64 (2015) 892.
[2] V.B. Yadava, R. Gadia, S. Kalra, Clay based nanocomposites for removal of heavy metals from water: a review, J. Environ. Manage., 232 (2019) 803–817.
[3] H.N.M.E. Mahmud, A.O. Huq, R. Binti Yahya, The removal of heavy metal ions from wastewater/aqueous solution using polypyrrole-based adsorbents, RSC Adv., 18 (2016) 14778–14791.
[4] H. Javadian, Application of kinetic, isotherm and thermodynamic models for the adsorption of Co(II) ions on polyaniline/polypyrrole copolymer nanofibers from aqueous solution, J. Ind. Eng. Chem., 20 (2014) 4233–4241.
[5] B. Samiey, C.H. Cheng, J. Wu, Organic-inorganic hybrid polymers as adsorbents for removal of heavy metal ions from solutions: a review, Materials, 7 (2014) 673–726.
[6] M.A. Renu, S. Kailash, S. Upadhyaya, R.K. Dohare, Removal of heavy metals from wastewater using modified agricultural adsorbents, Mater. Today:. Proc., 4 (2017) 10534–10538.
[7] S. Hydari, H. Sharififard, M. Nabavinia, M.R.A. Parvizi, Comparative investigation on removal performances of commercial activated carbon, chitosan biosorbent and chitosan/activated carbon composite for cadmium, Chem. Eng. J., 194 (2012) 276–282.
[8] Y.C. Sharma, V. Srivastava, V.K. Singh, S.N. Kaul, C.H. Weng, Nano-adsorbents for the removal of metallic pollutants from water and wastewater, Environ. Technol., 30 (2009) 583–609.
[9] A. Amari, M. Chlendi, A. Gannouni, A. Bellagi, Optimised activation of bentonite for toluene adsorption, Appl. Clay Sci., 47 (2010) 457–461.
[10] M. Auta, B.H. Hameed, Acid modified local clay beads as effective low-cost adsorbent for dynamic adsorption of methylene blue, J. Ind. Eng. Chem., 19 (2013) 1153–1161.
[11] A.K. Panda, B.G. Mishra, D.K. Mishra, R.K. Singh, Effect of sulphuric acid treatment on the physico-chemical characteristics of kaolin clay, Colloids Surf., A, 363 (2010) 98–104.
[12] E. Makó, Z. Senkár, J. Kristóf, V. Vágvölgyi, Surface modification of mechanochemically activated kaolinites by selective leaching, J. Colloid Interface Sci., 294 (2006) 362–370.
[13] C. Belver, M.A.B. Munoz, M.A. Vicente, Chemical activation of a kaolinite underacid and alkaline conditions, Chem. Mater., 14 (2002) 2033–2043.
[14] J. Madejova, FTIR techniques in clay mineral studies, Vib. Spectrosc., 31 (2003) 1–10.
[15] B.N. Dudkin, I.V. Loukhina, E.G. Avvakumov, V.P. Isupov, Application of mechnochemical treatment of disintegration of kaolinite with sulphuric acid, Chem. Sustainable Dev., 12 (2004) 327–330.
[16] R. Delhez, T.H. Keijser, E.J. Mittemeijer, E. Fresenius, Determination of crystallite size and lattice distortions through X-ray diffraction line profile analysis, Anal. Chem., 312 (1982) 1–10.
[17] H. Suquet, Effects of dry grinding and leaching on the crystal structure of chrysotile, Clays Clay Miner., 37 (1989) 439–445.

[18] K.K. Taha, M.S. Tagelsir, A.M. Musa, Performance of Sudanese activated bentonite in bleaching cotton seed oil, J. Bangladesh Chem. Soc., 24 (2011) 191–201.
[19] N. Hula, O. Muserret, S. Yukusel, The effect of sulphuric acid activation on crystallinity, surface area, porosity, surface acidity and bleaching power of bentonite, J. Food Chem., 105 (2007) 156–163.
[20] F. Hussin, M.K. Aroua, W.M.A.W. Daud, Surface chemistry and activation of bleaching earth: a review, Chem. Eng. J., 170 (2011) 90–106.
[21] A. Olgun, N. Atar, Equilibrium, thermodynamics and kinetic studies for the adsorption of lead(II) and nickel(II) onto clay mixture containing boron impurity, J. Ind. Eng. Chem., 18 (2012) 1751–1757.
[22] M. Auta, B.H. Hammed, Optimized waste tea activated carbon for adsorption of methylene blue and acid blue and acid blue 29 dyes using response surface methodology, Chem. Eng. J., 175 (2011) 233–243.
[23] L.G.T. Dos Reis, N.F. Robaina, W.F. Pacheco, R.J. Cassella, Separation of Malachite Green and Methyl Green cationic dyes from aqueous medium by adsorption on Amberlite XAD-2 and XAD-4 resins using sodium dodecylsulfate as carrier, Chem. Eng. J., 171 (2011) 532–540.
[24] N. Atar, A. Olgun, Removal of basic and acid dyes from aqueous solution, Desalination, 249 (2009) 109.
[25] F.D. Badii, M.A. Ardjani, N.Y. Saberi, S.Z. Limaee Shifaei, Adsorption of Acid Blue 25 on diatomite in aqueous solutions, Indian J. Chem. Technol., 17 (2010) 7–16.
[26] Y. Salameh, N. Al-Lagtah, M.N.M. Ahmad, S.J. Allen, G.M. Walker, Kinetic and thermodynamic investigations on arsenic adsorption onto dolomitic sorbents, Chem. Eng. J., 160 (2010) 440–446.
[27] I. Langmuir, The constitution and fundamental properties of solids and liquids, J. Am. Chem. Soc., 38 (1916) 2221–2295.
[28] H.M.F. Freundlich, Over the adsorption in solution, J. Physiochem., 57 (1906) 385–470.
[29] M.J. Temkin, V. Pyzhev, Recent modifications to Langmuir isotherms, Acta Physiochemical., 12 (1940) 217–225.
[30] N. Atar, A. Olgun, S. Wang, Adsorption of cadmium(II) and zinc(II) on boron enrichment process waste in aqueous solutions: batch and fixed-bed system studies, Chem. Eng. J., 192 (2012) 1–7.
[31] C.M. Futalan, C.C. Kan, M.L. Dalida, K.J. Hsien, C. Pascua, M.W. Wan, Comparative and competitive adsorption of copper, lead, and nickel using chitosan immobilized on bentonite, Carbohydr. Polym., 83 (2011) 528–536.
[32] M. Eloussaief, M. Benzina, Efficiency of natural and acid-activated clays in the removal of Pb(II) from aqueous solutions, J. Hazard. Mater., 178 (2011) 753–757.
[33] F. Sharifipour, S. Hojati, A. Landi, A. Faz Cano, Kinetics and thermodynamics of lead adsorption from aqueous solutions onto Iranian sepiolite and zeolite, Int. J. Environ. Res., 9 (2015) 1001–1010.
[34] A. Sdiri, K. Mohamed, B. Samir, E. Sherif, A natural clay adsorbent for selective removal of lead from aqueous solutions, J. Appl. Clay Sci., 126 (2016), 89–97.
[35] T. Wajima, Preparation of adsorbent with lead removal ability from paper sludge using sulfuric acid impregnation, APCBEE Procedia, 10 (2014) 164–169.
[36] A. Sdiri, T. Higashi, T. Hatta, F. Jamoussi, N. Tase, Evaluating the adsorptive capacity of montmorillonitic and calcareous clays on the removal of several heavy metals in aqueous systems, Chem. Eng. J., 172 (2011) 37–46.
[37] A. Salem, R. Akbari Sene, Removal of lead from solution by combination of natural zeolite–kaolin–bentonite as a new low-cost adsorbent, Chem. Eng. J., 174 (2011) 619–628.
[38] A. Sari, M. Tuzen, D. Citak, M. Soylak, Equilibrium, kinetic and thermodynamic studies of adsorption of Pb(II) from aqueous solution onto Turkish kaolinite clay, J. Hazard. Mater., 149 (2007) 283–291.
[39] A. Shahat, M.R. Awual, M.A. Khaleque, M.Z. Alam, M. Naushad, A.M.S. Chowdhury, Large-pore diameter nano-adsorbent and its application for rapid lead(II) detection and removal from aqueous media, Chem. Eng. J., 273 (2015) 286–295.
[40] V. Vetriselvi, R. Jaya Santhi, Redox polymer as an adsorbent for the removal of Chromium(VI) and lead(II) from the tannery effluents, Water Res. Ind., 10 (2015) 39–52.
[41] D. Tiwari, Lalhmunsiama, S.M. Lee, Iron-impregnated activated carbons precursor to rice hulls and areca nut waste in the remediation of Cu(II) and Pb(II) contaminated waters: a physico-chemical studies, Desal. Wat. Treat., 53 (2015) 1591–1605.
[42] S.M. Lee, C. Laldawngliana, D. Tiwari, Iron oxide nano-particles-immobilized-sand material in the treatment of Cu(II), Cd(II) and Pb(II) contaminated waste waters, Chem. Eng. J., 195–196 (2012) 103–111.
[43] Lalhmunsiama, S.M. Lee, D. Tiwari, Manganese oxide immobilized activated carbons in the remediation of aqueous wastes contaminated with copper (II) and lead (II), Chem. Eng. J., 225 (2013) 128–137.
[44] S. Lagergren, S.K. Svenska, On the theory of so-called adsorption of dissolved substances, Royal Swedish Acad. Sci. Doc., Band 24 (1898) 1–13.
[45] Y.S. Ho, S. McKay, Pseudo-second-order model for sorption processes, Process Biochem., 34 (1999) 451–465.
[46] S. Azizian, B. Yahyaei, Adsorption of 18-crown-6 from aqueous solution on granular activated carbon: a kinetic modeling study, J. Colloid Interface Sci., 299 (2006) 112–115.
[47] L.T. Nanganoa, J.M. Ketcha, J.N. Ndi, Kinetic and equilibrium modeling of the adsorption of amaranth from aqueous solution onto smectite clay, Res. J. Chem. Sci., 4 (2014) 7–14.
[48] S.S.M. Hassan, N.S. Awwad, H.A. Aboterika, Removal of synthetic reactive dyes from textile wastewater by Sorel's cement, J. Hazard. Mater., 162 (2009) 994–999.
[49] S. Hong, C. Wen, J. He, F. Gan, Y. Ho, Adsorption thermodynamics of Methylene Blue onto bentonite, J. Hazard. Mater., 167 (2009) 630–633.
[50] H. Aghdasinia, H.R. Asibi, Adsorption of a cationic dye (methylene blue) by Iranian natural clays from aqueous solutions: equilibrium, kinetic and thermodynamic study, Environ. Earth Sci., 77 (2018) 218.
[51] Q. Li, Q. Yue, Y. Su, B. Gao, H. Sun, Equilibrium, thermodynamics and process design to minimize adsorbent amount for the adsorption of acid dyes onto cationic polymer-loaded bentonite, Chem. Eng. J., 158 (2010) 489–449.
[52] T. Chen, T.Q. Zhang, T.H. Zhang, C.H. Gan, C.Y. Zheng, G. Yu, Carbon nanotube reinforced hydroxyapatite composite coatings produced through laser surface alloying, Carbon, 44 (2006) 37–45.
[53] F.N. Oskui, H. Aghdasinia, M.G. Sorkhabi, Adsorption of Cr(III) using an Iranian nanoclay: applicable to tannery wastewater: equilibrium, kinetic, and thermodynamic, Environ. Earth Sci., 78 (2019) 106.